

Two Distinct Binding Modes of a Protein Cofactor with its Target RNA

Gregory Bokinsky^{1,2}, Lucas G. Nivón^{1,3}, Shixin Liu^{1,2}, Geqing Chai⁵
Minh Hong^{1,2}, Kevin M. Weeks⁵ and Xiaowei Zhuang^{1,2,4*}

¹Howard Hughes Medical Institute, Harvard University Cambridge, MA 02138, USA

²Department of Chemistry and Chemical Biology, Harvard University, Cambridge MA 02138, USA

³Biophysics Program, Harvard University, Cambridge MA 02138, USA

⁴Department of Physics, Harvard University, Cambridge MA 02138, USA

⁵Department of Chemistry University of North Carolina Chapel Hill, NC 27599, USA

*Corresponding author

Like most cellular RNA enzymes, the bI5 group I intron requires binding by a protein cofactor to fold correctly. Here, we use single-molecule approaches to monitor the structural dynamics of the bI5 RNA in real time as it assembles with its CBP2 protein cofactor. These experiments show that CBP2 binds to the target RNA in two distinct modes with apparently opposite effects: a “non-specific” mode that forms rapidly and induces large conformational fluctuations in the RNA, and a “specific” mode that forms slowly and stabilizes the native RNA structure. The bI5 RNA folds through multiple pathways toward the native state, typically traversing dynamic intermediate states induced by non-specific binding of CBP2. These results suggest that the protein cofactor-assisted RNA folding involves sequential non-specific and specific protein–RNA interactions. The non-specific interaction potentially increases the local concentration of CBP2 and the number of conformational states accessible to the RNA, which may promote the formation of specific RNA–protein interactions.

© 2006 Elsevier Ltd. All rights reserved.

Keywords: ribonucleoprotein; RNA–protein interaction; RNA folding; group I intron; FRET

Introduction

Ribonucleoprotein (RNP) complexes catalyze many essential cellular reactions, including important examples such as protein synthesis and messenger RNA processing. In these RNPs, the catalytic site is often formed by the RNA while the protein cofactors play auxiliary roles.¹ These enzymatic RNAs must fold to specific structures to function properly. *In vitro*, RNA folding tends to be difficult for two reasons: the energy landscape of the RNA is rugged with kinetic traps that prevent efficient folding or the active state of the RNA is only marginally stable.^{2–15} In cells, these difficulties are mitigated in part by the association of RNA with protein cofactors that facilitate RNA folding.^{12–15}

Proteins appear to facilitate the folding of RNA *via* two broad mechanisms.^{12,13} In the first mechanism,

proteins interact non-specifically with the RNA and promote RNA folding by resolving non-native conformations, in a way analogous to chaperones acting on misfolded proteins.^{13,16,17} The non-specific nature of these RNA–protein interactions may also inhibit RNA folding under certain conditions, by disrupting native RNA structures as well as misfolded ones. In a second mechanism, a specific protein cofactor binds to well-defined structural features of its target RNA, stabilizing the native RNA structure. If the protein cofactor binds to the RNA at an early step in the folding pathway, the protein may effectively nucleate subsequent RNA folding.^{11,18} Alternatively, the protein cofactor may capture and stabilize a transiently formed native RNA structure, rather than actively inducing structural changes in the RNA, a mechanism referred to as tertiary structure capture. This has been thought to be the mechanism by which CBP2 facilitates the folding of the yeast mitochondrial bI5 group I intron.^{19,20} A protein cofactor may also facilitate RNA folding by a mechanism that exhibits features of both tertiary structure nucleation or capture.^{21,22} An RNA molecule could also rely on both a chaperone and a distinct specific cofactor working in concert to

Abbreviations used: RNP, ribonucleoprotein; FRET, fluorescence resonance energy transfer.

E-mail address of the corresponding author: zhuang@chemistry.harvard.edu

accomplish efficient folding.²³ The level of complexity observed for protein-facilitated RNA folding makes the acquisition of real-time information on folding dynamics critical for a comprehensive understanding of folding mechanisms.

In this work, we use fluorescence resonance energy transfer (FRET)^{24,25} to investigate the real-time folding dynamics of RNP complexes at the single-molecule level. It has been shown that single-molecule FRET can be used to detect conformational changes in a small RNA three-helix junction induced by a specific ribosomal protein and in a DNA stem-loop induced by an RNA chaperone.^{26,27} A useful property of the single-molecule approach is its ability to detect non-accumulative folding intermediates and multiple folding pathways that are potentially difficult to detect in ensemble measurements.^{6,28–31} Here, we report a dynamic structure for the bI5 group I intron RNA and two binding modes between this RNA and its protein cofactor, CBP2. While the specific CBP2–RNA binding mode stabilizes native RNA structures, the non-specific binding mode of CBP2 causes large conformational fluctuations in the RNA. Before attaining its native structure, the bI5 RNA folds through fluctuating intermediate states induced by non-specific CBP2 binding. These results suggest a complex assembly mechanism that involves both non-specific and specific interactions by a protein cofactor with its RNA target, which ultimately lead to formation of a well-defined and active state.

Results

Preparation of bI5 for investigation by single-molecule FRET

The bI5 RNP is comprised of the bI5 group I intron RNA and its CBP2 protein cofactor. The bI5 RNA

exhibits splicing activity while CBP2 facilitates folding of the RNA.^{10,32–34} The bI5 RNA contains three major domains: the P5–P4–P6 and P7–P3–P8 domains, which constitute the conserved catalytic core of all group I introns, and the 5' domain, which spans helices P1–P2–P2a (Figure 1(a)).

To probe the folding of bI5 molecules with FRET, we attached FRET donor (Cy3) and acceptor (Cy5) dyes near the 5' and 3' splice sites, respectively (Figure 1(a)). The efficiency of energy transfer from donor to acceptor is sensitive to the relative positions of the two dye molecules. Measurements of the energy transfer efficiency thus allow us to monitor the folding of the RNA to the native state, which should exhibit a high FRET efficiency due to the close proximity of the splice sites. Here, we analyze the bI5 RNA at various Mg^{2+} concentrations, primarily focusing on 7 and 40 mM Mg^{2+} . Distinct structures of the RNA were previously identified under these conditions, facilitating the assignment of observed FRET values to specific structural states of the bI5 RNA.^{10,35} To follow conformational dynamics of individual molecules in real time, the RNA was immobilized through a DNA tether to a surface *via* a biotin–streptavidin linkage. The surface was coated with polyethylene glycol to prevent non-specific protein interactions with the surface (see Figure 1 in Supplementary Data).³⁶ Fluorescence emission from single bI5 RNA molecules was detected using a total-internal-reflection microscope.

The labeling scheme allows us to monitor the splicing activity of the CBP2–bI5 RNP. Upon addition of guanosine monophosphate (GMP) to the pre-folded CBP2–bI5 complex, the 5' and 3' exons are brought together and the Cy3 and Cy5 dyes are spliced into close proximity to yield a high FRET signal (Figure 1(a) and (b)). We monitor the splicing reaction of individual surface-immobilized RNP complexes and measure the rate of accumulation of

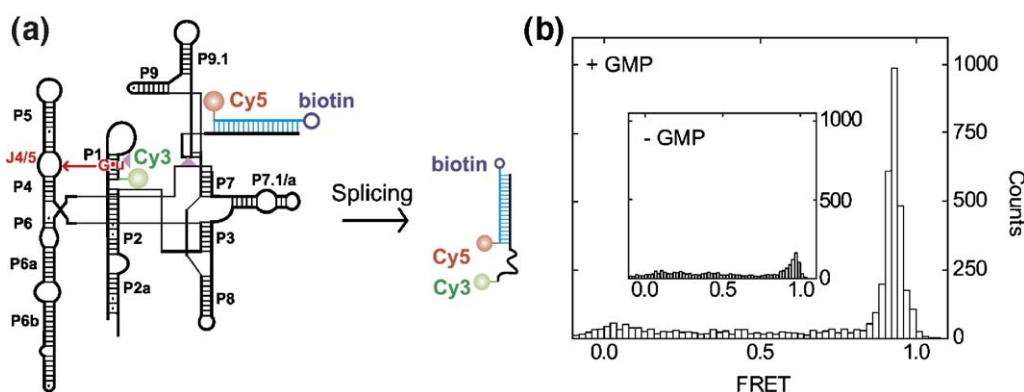


Figure 1. The bI5 construct used for single-molecule FRET experiments and its self-splicing reaction. (a) Secondary structure of the bI5 group I intron RNA and its splicing product. Splice sites are marked with purple triangles. The G–U wobble pair and its interaction with the J4/5 junction is marked in red. The biotinylated DNA tether is shown in blue. Splicing was initiated by 2 mM GMP and the resulting close proximity between FRET donor (Cy3) and acceptor (Cy5) in the spliced product leads to a high FRET efficiency, as shown in (b). After adding a stop solution containing EDTA and Proteinase K, only the spliced products show FRET=0.9, while the unspliced RNA molecules primarily show no fluorescence signal due to dissociation of the Cy3-labeled RNA strand in the absence of Mg^{2+} . Inset: Minimal spliced products observed in the absence of GMP.

the splice product. The observed reaction rate and extent are in quantitative agreement with those obtained from ensemble solution-phase measurements of bI5 RNPs (Figure 2(a) and (b)). These rates are also similar to the splicing rate for constructs without dyes, but moderately faster than the rate of the unmodified RNP lacking the DNA tether (Figure 2(c)), suggesting that hybridization with the DNA tether removes an interfering effect of the 3' exon on the splicing activity of the intron. Together, these results indicate that the surface-tethered RNA construct used here is a good model system for the bI5 RNA.

Structural dynamics of the bI5 RNA in the absence of CBP2

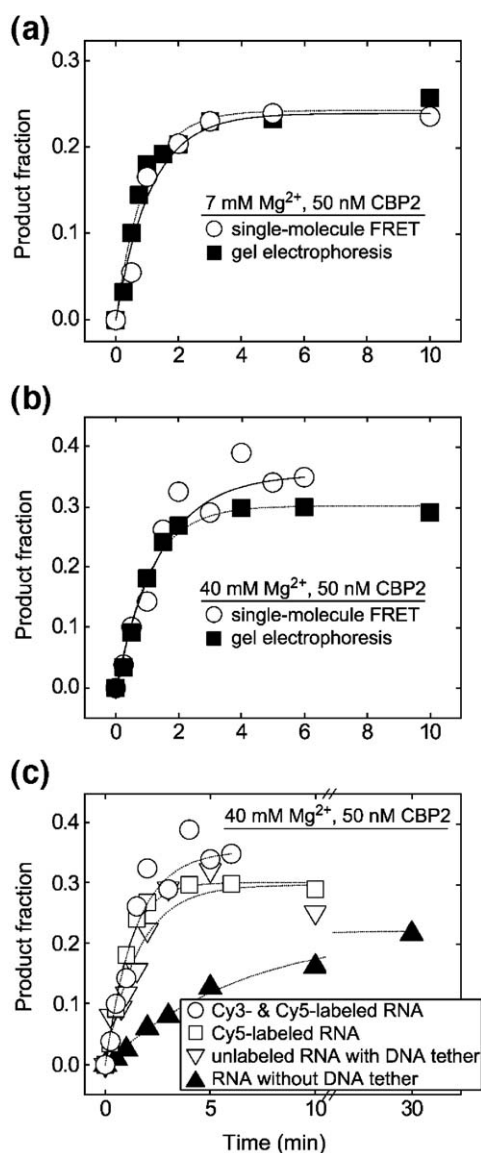
In the absence of CBP2, the single-molecule FRET trajectories of the bI5 RNA show stochastic transitions between two FRET levels (Figure 3). At 7 mM Mg^{2+} , a near-physiological ionic environment, the two levels are centered at 0.3 and 0.8, respectively (Figure 3(a)). The equilibrium constant between the 0.8 and 0.3 levels is 0.12, and the forward and backward switching rate constants are 0.25 s^{-1} and 1.9 s^{-1} , respectively (see Figure 2 in Supplementary Data). As the Mg^{2+} concentration increases, the value of the lower FRET level increases (Figure 3(c)) while that of the higher FRET level remains unchanged. The equilibrium shifts toward the higher FRET state (Figure 3(d)).

To assign the two folding states of the bI5 RNA, we monitored the FRET signal of both our primary construct (Figure 1(a)) and a truncated construct, $\Delta P1-P2$, which lacks the P1-P2 domain but can fold

independently (see Figure 6(a), below).³⁵ The Cy5 positions are identical in the two constructs; the Cy3 positions are also similar in the context of the RNA secondary structure. Like the original bI5 RNA, FRET trajectories of the $\Delta P1-P2$ construct predominantly dwell at FRET=0.3, but now switch to the higher FRET level only rarely. The lower FRET level of the $\Delta P1-P2$ construct also increases with Mg^{2+} concentration, with a trend very similar to that observed for the conformational collapse and core formation of the $\Delta P1-P2$ construct previously monitored by electrophoretic mobility and size exclusion chromatography (compare filled squares with open circles, Figure 3(c)).³⁵ From this, we infer that the lower FRET level corresponds to conformational collapse and core formation of the bI5 RNA.

To identify the structural change associated with the excursions to a higher FRET level (FRET=0.8), we mutated the G-U wobble base-pair in the P1 helix to a G-C Watson-Crick base-pair (the U-1C mutation). This mutation disrupts a

Figure 2. Similar splicing kinetics for the bI5 RNA as measured by single-molecule and ensemble measurements. (a) Splicing kinetics in 7 mM Mg^{2+} , 50 nM CBP2 and 2 mM GMP determined with single surface-immobilized molecules (open circles, FRET assay, $0.9(\pm 0.2)\text{ min}^{-1}$) are the same as those determined for freely diffusing bI5 RNA (filled squares, gel electrophoresis assay, $1.1(\pm 0.1)\text{ min}^{-1}$). Non-specifically bound and excess CBP2 was removed by addition of 100 $\mu\text{g}/\text{ml}$ of heparin and 2 mM GMP. (b) Splicing kinetics measured in 40 mM Mg^{2+} , 50 nM CBP2 determined with single surface-immobilized molecules (open circles, $1.0(\pm 0.1)\text{ min}^{-1}$) and with freely diffusing bI5 RNA (filled squares, $0.7(\pm 0.1)\text{ min}^{-1}$). No heparin was added to remove non-specifically bound CBP2 in this case. (c) Splicing kinetics for four different bI5 constructs in 40 mM Mg^{2+} , 50 nM CBP2. The splicing rate constant for the Cy3 and Cy5-labeled constructs depicted in Figure 1(a) (open circles, $1.0(\pm 0.1)\text{ min}^{-1}$) is similar to that of a bI5 construct without the Cy3 dye but with Cy5 dye still present on the DNA tether (open squares, $0.7(\pm 0.1)\text{ min}^{-1}$) and to that of a construct omitting the Cy5 dye from the DNA tether (open triangles, $0.6(\pm 0.2)\text{ min}^{-1}$). The splicing rate constant of a bI5 construct that lacks the DNA tether is significantly slower (filled triangles, $0.16(\pm 0.02)\text{ min}^{-1}$), suggesting that hybridization of the DNA tether to the 3' exon removes an interfering effect of the 3' exon on the splicing activity of the intron.



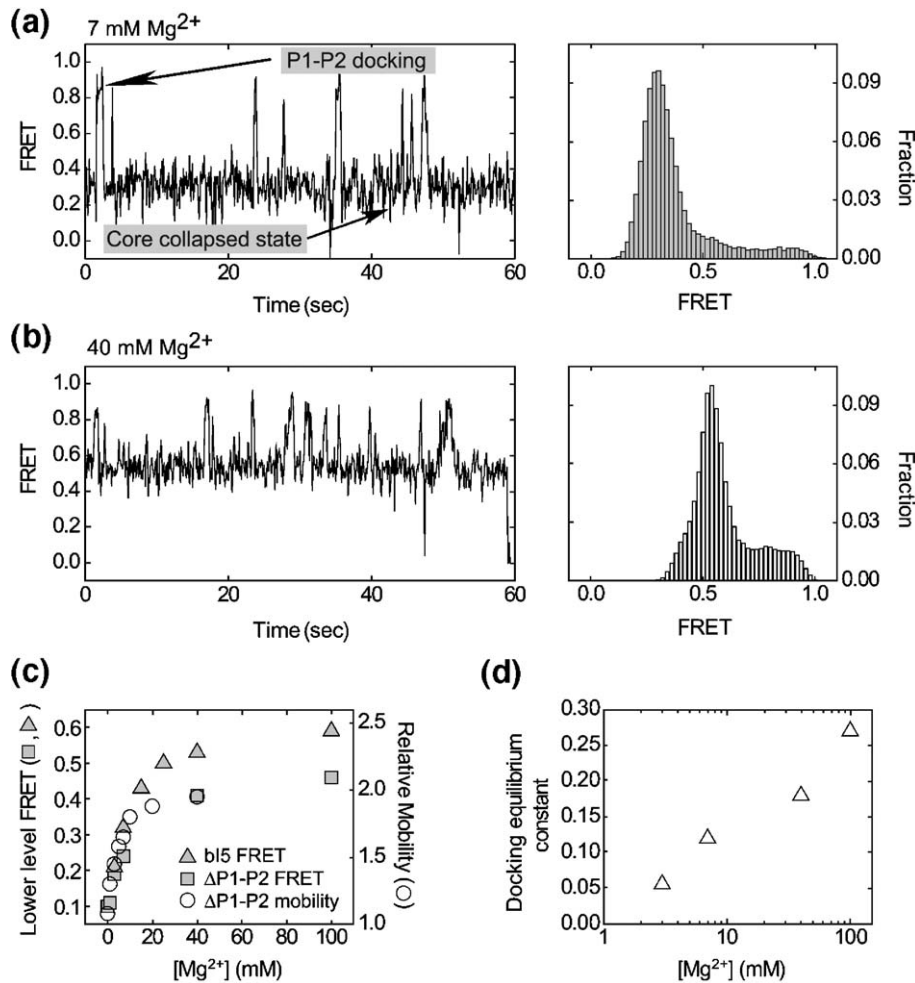


Figure 3. Structural dynamics of the bI5 RNA in the absence of CBP2. (a) and (b) FRET trajectories of single molecules (left) and a histogram constructed from many bI5 RNA molecules (right) in 7 and 40 mM Mg²⁺. In constructing the histogram, a threshold is applied to remove FRET values associated with either blinking or photobleaching of Cy5. (c) The dependence of the lower FRET level as a function of Mg²⁺ concentration for the bI5 (filled triangles) and bI5 Δ P1-P2 (filled squares) constructs. Overlaid is the electrophoretic mobility of the bI5 Δ P1-P2 construct (open circles).³⁵ (d) Equilibrium constant for the formation of the higher FRET states.

tertiary contact between the P1 helix and the A-rich loop in the J4/5 region in the catalytic core of the bI5 RNA (Figure 1(a)).^{37,38} While switching between the same high and low levels is still observed, the U-1C mutation shifts the equilibrium significantly toward the lower FRET level, reducing the equilibrium constant from 0.12 to 0.03 at 7 mM Mg²⁺. This suggests that the FRET=0.8 state is at least partially stabilized by the tertiary interaction between the P1 helix and the bI5 core, and the appearance of this state is primarily due to the docking of the P1-P2 domain into the bI5 core. Consistent with this picture, removal of the P1-P2 domain also reduces the equilibrium constant to 0.03 at 7 mM Mg²⁺.

The above data suggest a structural picture for the collapsed state in which the RNA tends to form short-lived structures with native-like features. This is consistent with previous results that the bI5 RNA forms a collapsed state with native-like topology at 7 mM Mg²⁺.^{35,39} However, in the absence of CBP2 7 mM Mg²⁺, little splicing activity was observed despite

prolonged incubation with GMP (30 min), indicating that the high FRET state observed here is non-native, either because the catalytic core is not accurately folded, or because the P1-P2 domain is not accurately docked with the core.

Two binding modes of CBP2 lead to distinct conformational changes in the RNA

The conformational dynamics of the bI5 RNA change dramatically when CBP2 binds. At 7 mM Mg²⁺, two types of single-molecule FRET trajectories occur upon binding by CBP2 (Figure 4). The first type (type I) exhibits regular, stepwise transitions between two FRET levels (Figure 4(a)). Whereas the higher level remains at 0.8, the lower level is now centered at 0.5, significantly higher than that observed for the CBP2-free RNA at 7 mM Mg²⁺ (compare with Figure 3(a)). The second type (type II) exhibits broad and irregular fluctuations that are no longer primarily stepwise,

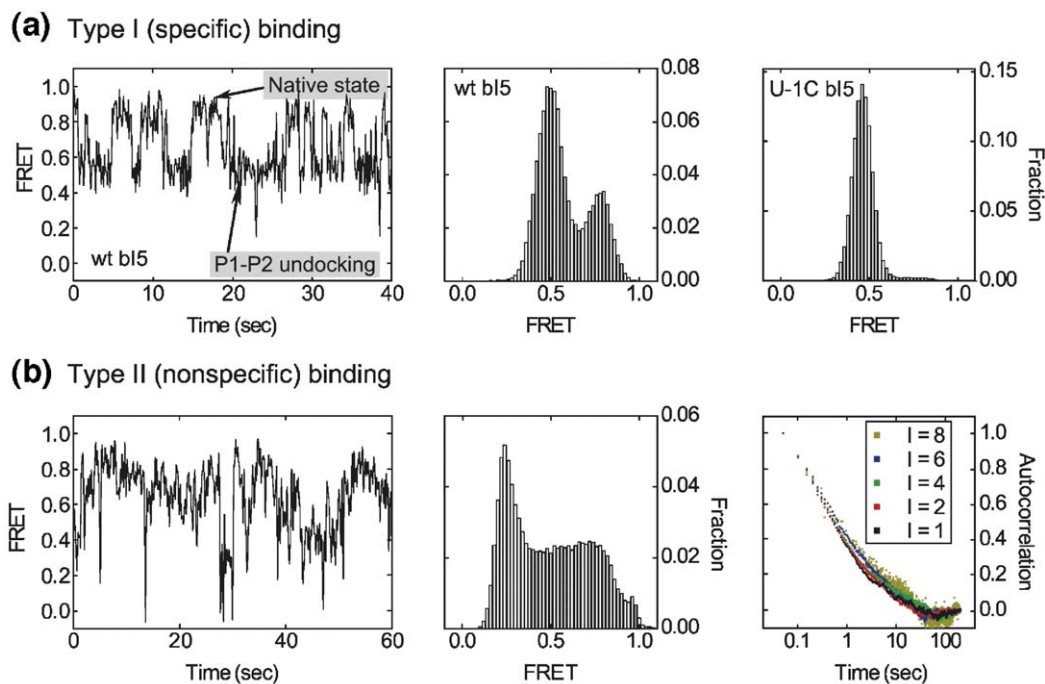


Figure 4. CBP2 binds to the bI5 RNA in two modes, each inducing distinct conformational dynamics in bI5 RNA. (a) Specific binding of CBP2 stabilizes the native structure of the bI5 RNA. Left panel: FRET trajectory of a bI5 RNA specifically bound to CBP2 in 7 mM Mg^{2+} showing regular transitions between FRET levels of 0.5 and 0.8 (type I binding behavior). Center panel: FRET histogram of many specific CBP2–bI5 RNA complexes. Right panel: FRET histogram of U-1C mutant molecules specifically bound to CBP2. The regular transitions between FRET=0.5 and 0.8 are used as a signature for identifying specific binding. (b) Non-specific binding by CBP2 induces large conformational fluctuations in the bI5 RNA. Left panel: FRET trajectory of a bI5 RNA molecule in 7 mM Mg^{2+} and 50 nM CBP2, depicting broad and continuous fluctuations across a wide range of FRET values (type II binding behavior). Center panel: FRET histogram obtained from all CBP2–bI5 complexes in 7 mM Mg^{2+} and 50 nM CBP2. Right panel: Autocorrelation function constructed from many FRET trajectories at five laser intensities (I , in arbitrary units).

but often appear continuous (Figure 4(b)). While both types of behavior co-exist among the RNA molecules at very low CBP2 concentrations, the type II behavior dominates at CBP2 concentrations above 5 nM (Figure 5(a)). Moreover, the overall amplitude of type II fluctuations increases with the CBP2 concentration and the FRET values adopt a very broad distribution ranging from 0.1 to 0.9 at high CBP2 concentrations (Figure 4(b)). The fluctuations also occur over a wide range of timescales. The autocorrelation spectrum of the FRET trajectories, which measures the rate of FRET fluctuations, cannot be fit to first-order kinetics with a single rate constant, but instead spans three orders of magnitude in time, from 0.05 s to 30 s (Figure 4(b)). The autocorrelation spectrum is independent of the laser intensity used, indicating that the FRET fluctuations are not due to photophysical effects of the dyes.

When the bI5 RNA is first incubated with a high concentration of CBP2 so that the majority of FRET trajectories exhibit the type II behavior and is then buffer-exchanged to remove CBP2 in the solution, the FRET trajectories convert to the type I behavior at the relatively slow rate of 0.04 min^{-1} (see Figure 3 in Supplementary Data). This conversion rate is far slower than the FRET fluctuation rates observed in

the type II behavior (Figure 4(b)), suggesting that type II fluctuations are not due to rapid binding and dissociation of CBP2 from the RNA. This is also supported by the observation that type II fluctuations persist with similar amplitude for a sustained period of time after buffer exchange, despite the absence of excess CBP2 available in the solution to bind the RNA (data not shown). Interestingly, addition of a tRNA or heparin competitor appears to destabilize type II binding, accelerating the conversion to the type I behavior by about tenfold (Supplementary Data, Figure 3). Dissociation of CBP2 bound in type I mode is slow. A thorough removal of the stably bound CBP2 by addition of Proteinase K converts the FRET dynamics to those indicative of CBP2-free RNA, which exhibits step-wise FRET transitions between 0.3 and 0.8.

These experiments suggest that type I behavior (Figure 4(a)) is due to strong binding of CBP2, whereas type II behavior (Figure 4(b)) is due to weaker and presumably less specific binding by CBP2 to the RNA, which can be readily disrupted by competitors. In the following, we operationally refer to type I and II CBP2 binding as “specific” and “non-specific” binding, respectively. These two binding modes are not necessarily mutually exclusive. The decreases in the type I fraction seen at high CBP2

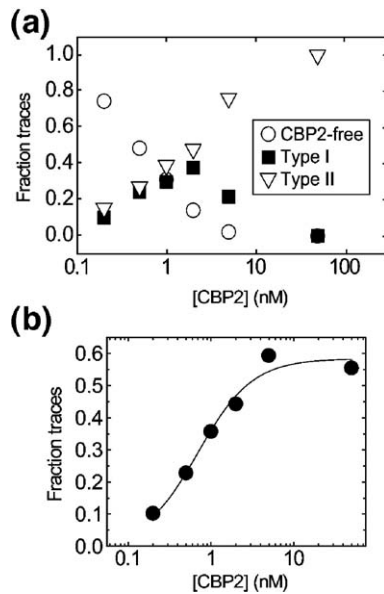


Figure 5. Concentration dependence of the two CBP2 binding modes. (a) Fractions of RNA molecules not bound to CBP2 (open circles), bound to CBP2 in the type I mode (filled squares) or the type II mode (open triangles) as a function of CBP2 concentration. (b) Fraction of molecules exhibiting the specific (type I) binding mode after incubation with 50 nM CBP2 for 30 min followed by treatment with 100 $\mu\text{g}/\text{ml}$ of heparin for about 5 min to remove non-specifically bound CBP2 from the RNA. The data are fit to $A[\text{CBP2}]^n/([\text{CBP2}]^n + K^n)$ with a Hill coefficient, $n = 1.3 \pm 0.3$.

concentrations (Figure 5(a)) do not necessarily indicate replacement of specifically bound CBP2 by non-specifically bound CBP2, but instead CBP2 bound in both modes may coexist on the same RNA at these concentrations with the type I dynamics masked by the type II FRET fluctuations.

Specific binding of CBP2 stabilizes the native tertiary contacts in the bI5 RNA

In the native CBP2–bI5 complex, a single CBP2 protein remains strongly bound to the bI5 RNA molecule in the presence of heparin.^{20,33} To determine the stoichiometry of the specifically bound CBP2, we performed a titration of bI5 with CBP2, followed by treatment with heparin to remove non-specific binding. The fraction of molecules with type I behavior can be fit with a Hill coefficient close to 1 ($n = 1.3 \pm 0.3$; Figure 5(b)), suggesting that specific binding can be accounted for by binding of a single CBP2 molecule.

At 7 mM Mg^{2+} , the lower FRET level increases upon specific CBP2 binding from 0.3 to 0.5, a value similar to the lower FRET level exhibited at 40 mM Mg^{2+} without CBP2 (compare Figure 4(a) with Figure 3(b)). This is consistent with a previous model suggesting that both CBP2 and high concentrations of Mg^{2+} tend to promote the formation of the bI5 RNA core.¹⁰ Furthermore, the equilibrium constant between the 0.8 and the lower FRET levels

increases from 0.12 to 0.49 upon specific binding of CBP2 (compare Figure 4(a) with Figure 3(a)). The U-1C mutation, which disrupts a tertiary contact between the P1 helix and the bI5 core, reduces the equilibrium constant from 0.49 to 0.02 (Figure 4(a)). This mutation also eliminates splicing activity whereas native sequence CBP2–bI5 complexes are catalytically active at 7 mM Mg^{2+} (Figure 2(a)). We thus infer that the FRET=0.8 state observed in the specific binding mode is the native state of the bI5 RNP with the P1–P2 domain docked into the catalytic core and that the transitions observed between 0.5 and 0.8 FRET levels indicate docking and undocking of P1–P2. These results show that specific CBP2 binding strongly promotes P1–P2 docking.

Non-specific binding of CBP2 causes dynamic structural fluctuations in the RNA

The type II binding mode of CBP2 induces broad fluctuations in FRET that span nearly the entire observable FRET range and a few orders of magnitude in time (Figure 4(b)). To distinguish whether these fluctuations report conformational changes in the RNA or changes in the photophysical properties of the dyes induced by potential interactions of CBP2 with the dyes, we designed two control bI5 constructs in which the FRET donor and acceptor are linked *via* a perfectly base-paired duplex. In these constructs, the inter-dye distance cannot change, thus changes in FRET arising from conformational changes of the RNA should be eliminated but potential CBP2-induced changes in the photophysical properties of the dyes should remain (see Supplementary Data, Figure 4). FRET trajectories for both control constructs demonstrate a steady FRET signal except for abrupt transitions to FRET=0 caused by blinking of the acceptor dye, a well-known photophysical phenomenon. Thus, the observed broad FRET fluctuations between non-zero values (Figure 4(b)) largely report authentic conformational dynamics of the bI5 RNA. These results, together with the observation that the FRET fluctuation rates are much faster than the CBP2 dissociation rate, indicate that the observed FRET fluctuations are due to conformational fluctuations of the bI5 RNA while CBP2 proteins remain bound.

Next we evaluate which domains of the RNA fluctuate when bound by CBP2 in the type II mode. A possible origin for the conformational fluctuations arises from the peripheral domains P1–P2 and P9–P9.1, which are connected to the catalytic core *via* relatively long, potentially flexible, single-stranded regions. To test this idea, we deleted the P1–P2 or P9–P9.1 domains from the primary construct (Figure 6(a) and (b)). In these truncated constructs, we still observe broad, irregular FRET fluctuations, albeit with fluctuation amplitudes that are moderately smaller than those observed in the original RNA. Remarkably, even the double-deletion construct bI5 $\Delta\text{P1-P2} \Delta\text{P9-P9.1}$, which

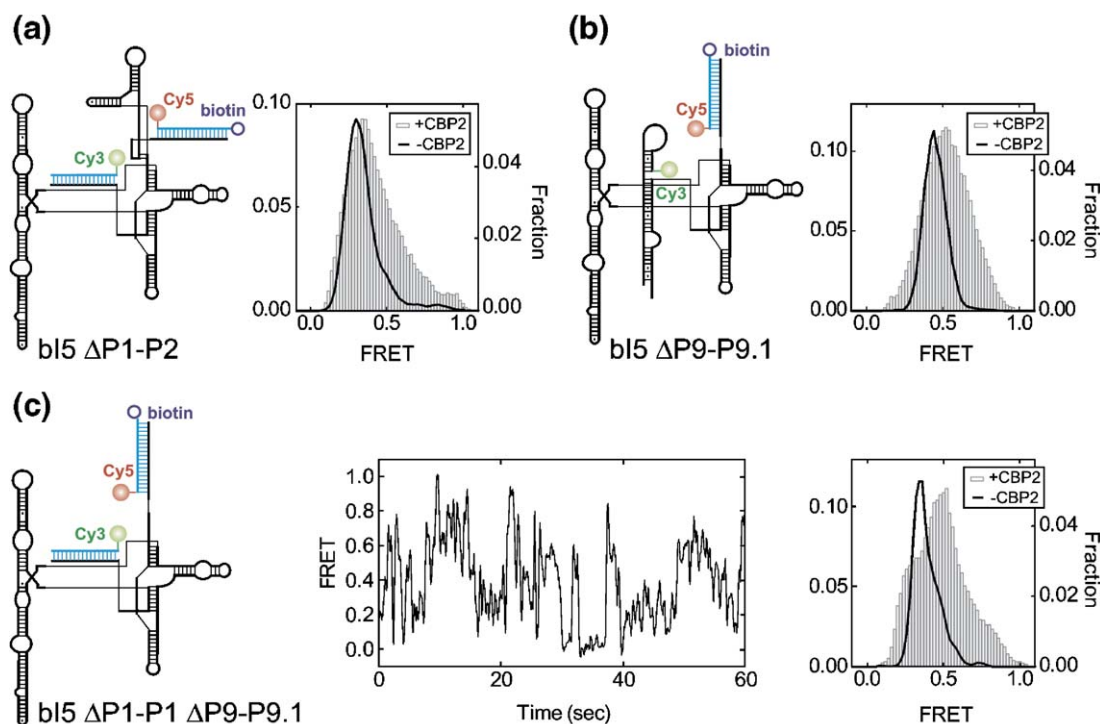


Figure 6. CBP2 induces broad structural fluctuations in diverse bI5 RNA variants. (a) and (b) $\Delta P1-P2$ and $\Delta P9-P9.1$ constructs. The FRET histograms were constructed from many RNA molecules in 7 mM Mg^{2+} and 50 nM CBP2. (c) The minimum bI5 core with both P1-P2 and P9-P9.1 peripheral domains deleted. A single RNA molecule FRET trajectory in 7 mM Mg^{2+} and 50 nM CBP2 and a FRET histogram constructed from many molecules are shown. In all cases, the FRET histograms of the constructs in 7 mM Mg^{2+} in the absence of CBP2 are overlaid for comparison (continuous lines).

contains only the minimum core spanning the P5-P4-P6 and P7-P3-P8 domains, exhibits significant CBP2-induced fluctuations (Figure 6(c)), suggesting that CBP2 possesses a robust ability to induce RNA structural fluctuations.

To determine if binding of CBP2 can disrupt Watson-Crick base-pairs, a basic RNA structural motif, we designed a simple RNA construct that consists of an AU-rich hairpin labeled with a donor and acceptor (Figure 7). We expect that melting of the hairpin will decrease FRET efficiencies as the dyes are pulled apart. CBP2-induced fluctuations to lower FRET values are indeed observed (Figure 7(a)), whereas a structurally similar control construct with the two dyes covalently confined to within two nucleotide bases does not exhibit such fluctuations (Figure 7(b)), suggesting that CBP2 is capable of melting RNA secondary structures.

The structure-destabilizing properties of non-specific CBP2 binding suggest that under conditions where non-specific binding dominates, native RNA contacts might also be disrupted. Consistent with this notion, we find that high concentrations of CBP2 partially inhibit splicing at low Mg^{2+} concentrations. At 7 mM Mg^{2+} and 10 nM CBP2, a condition at which most RNA molecules exhibit non-specific CBP2 binding (see Figure 5), splicing is eightfold slower than the rate measured in the presence of heparin to remove non-specific binding. This inhibitory effect is not observed at high Mg^{2+} concentrations.

Binding by CBP2 is fast and follows bimolecular kinetics

The addition of CBP2 to the bI5 RNA changes the RNA conformational dynamics rapidly. The transition from the two-state behavior of the free RNA to the broad, continuous fluctuation behavior characteristic of the type II CBP2 binding occurs with a rate constant of 12 min^{-1} upon addition of 50 nM CBP2 (Figure 8(a) and (b)). This binding rate scales linearly with CBP2 concentration (Figure 8(c)). This result shows that formation of the non-specific CBP2–bI5 RNA complex follows simple, concentration-dependent, bimolecular kinetics with a rate constant close to the diffusion-limit ($6 \times 10^8 \text{ M}^{-1} \text{ min}^{-1}$).

In contrast, as judged by nitrocellulose filter partitioning, splicing activity, and time resolved footprinting assays, the assembly of stable, functional bI5 RNPs exhibits slow, protein-concentration-independent, unimolecular kinetics (0.5 min^{-1}).^{19,40,41} Even the formation of a stable, non-functional complex between CBP2 and an expanded, non-native bI5 RNA state that forms in the absence of Mg^{2+} follows slow, unimolecular kinetics.²⁰ Considering that the dissociation kinetics of type II binding mode makes it difficult to detect in these bulk assays, the above results, taken together, suggest that formation of the CBP2–bI5 RNA complex occurs in two major steps. First, a non-specific CBP2–RNA encounter complex forms *via* a fast, bimolecular step and induces substantial conformational fluctuations in the RNA. This rapid

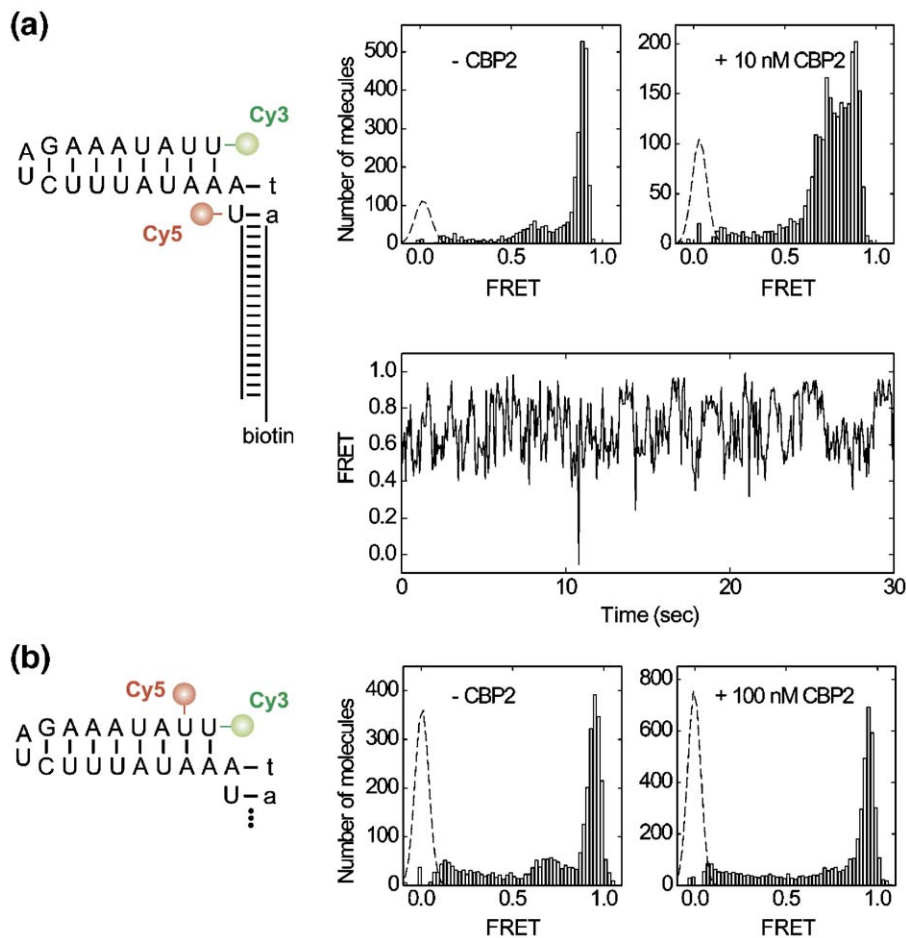


Figure 7. CBP2 binding destabilizes RNA base-pairs and causes conformational fluctuations in an RNA hairpin. (a) RNA hairpin construct, SL1, labeled with a fluorescent Cy3 donor and Cy5 acceptor. Top panels: The FRET histogram of the RNA hairpin indicates that most of the molecules exhibit a well-defined FRET value with a sharp peak at 0.9 as expected for well-formed hairpins. The small peak at FRET \sim 0.7 may be due to a misfolded form. Upon addition of CBP2, the FRET distribution broadens significantly due to fluctuations toward lower FRET values. A typical trajectory showing such fluctuations is displayed in the lower panel. (b) Control construct, SL1PC, designed to test the potential effect of dye–CBP2 interaction in which the Cy3 and Cy5 dyes are placed on adjacent nucleotides. In this case, CBP2 does not induce broadening of the FRET profile. For clarity, the peak at FRET=0, reflecting inactive or blinking Cy5 (dash line), has been subtracted from the experimentally determined histogram. These data were recorded in 10 mM NaCl, 10 mM Hepes (pH 7.6), and the oxygen scavenger system as described in Methods.

step is then followed by slow formation of a stronger and specific CBP2-bI5 complex.

bI5 folding occurs through multiple pathways and dynamic intermediate states

Next, we investigated the transient assembly dynamics of the bI5 RNA to a native RNP initiated by a buffer containing high concentrations of Mg^{2+} (40 mM) and CBP2 (50 nM). Under these conditions, the bI5 RNA is fully active (Figure 2(b)). The FRET trajectories dwell predominantly at a high level of 0.8, and exhibit brief but frequent fluctuations towards lower values at around 0.6 (Figure 9(a)). The U-1C mutation, which destabilizes the P1-P2 docking and eliminates splicing activity, greatly reduces the docking equilibrium so that the molecules predominantly dwell at the lower FRET level of 0.6 (Figure 9(b)). These observations indicate that

the FRET=0.8 state observed here is the native state of the bI5 RNA with the P1-P2 domain docked into the bI5 core.

To observe the folding process in real time, we prepared the bI5 RNA without CBP2 in 7 mM Mg^{2+} , a condition at which few stable tertiary contacts are formed,^{10,35,39} and initiated folding by addition of a buffer containing 40 mM Mg^{2+} and 50 nM CBP2. The majority of molecules (65%) reach the native state within our observation time, as recognized by a persistent high FRET level of 0.8 (Figure 9(c)). Among the molecules that reach a sustained FRET level of 0.8, 70% exhibit splicing activity, as determined by the assay described in Figure 1. This is consistent with the previously observed fraction (60%–70%) of bI5 RNPs being catalytically active, among which about 60% produce splice product and 40% only yield 5' cleavage product.³³ Remarkably, before attaining the native state, most molecules traverse a highly

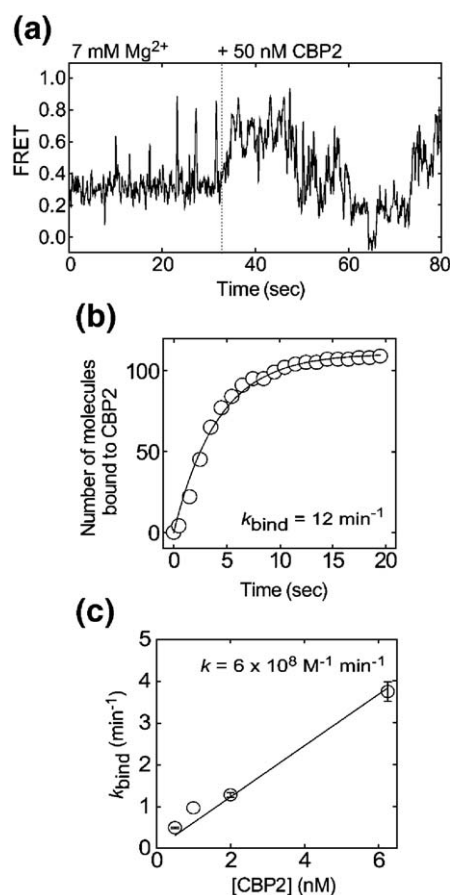


Figure 8. CBP2 binds rapidly to the bI5 RNA with bimolecular kinetics. (a) Trajectory showing rapid conversion of the free bI5 RNA to CBP2 bound state after addition of 50 nM CBP2 (dotted line). (b) Number of bI5 RNA molecules bound by CBP2 as a function of time. CBP2 binding time is scored as the time when the FRET trajectory shows the broad irregular fluctuations. A single-exponential fit gives a binding rate of 12 min^{-1} . The binding rate constant can also be determined from the average FRET value for an ensemble of bI5 molecules, yielding similar results (data not shown). (c) Binding rate constants as a function of CBP2 concentration. The slope of this line gives the second order rate constant.

dynamic ensemble of intermediate states (Figure 9(c)), which exhibit broad, irregular fluctuations that are similar to the conformational fluctuations induced by non-specifically bound CBP2 at 7 mM Mg^{2+} (Figure 4(b)). The bI5 molecules traverse a multitude of pathways as they fold to the native state, clearly indicated by different transient folding dynamics observed in individual FRET trajectories. By recording the time at which each molecule acquires the native state, we obtained a folding time course that is described by at least two rate constants, 0.5 and 7 min^{-1} (Figure 9(d)), further evidence for the existence of multiple folding pathways. Similar folding kinetics are obtained when the bI5 RNA is pre-incubated with 40 mM Mg^{2+} before folding is initiated by the addition of 50 nM CBP2 (Figure 9(d)). This indicates that the rate-limiting step for bI5

folding is not the structural transition induced by increasing the Mg^{2+} concentration from 7 mM to 40 mM, but instead occurs at a later stage during the protein-dependent folding process. In the presence of heparin to compete with RNA for CBP2 binding, folding kinetics are significantly slower (see Figure 5 in Supplementary Data). This could result from a reduction in non-specific bI5-CBP2 binding, which may in turn promote the RNA folding and the assembly of specific RNA-CBP2 complexes, or from a kinetic inhibition of specific bI5 RNA-CBP2 interactions directly by heparin.

Discussion

Nearly all cellular RNA enzymes rely on the help of proteins that bind either specifically or non-specifically in order to function properly. In many cases, the role of these proteins is to help the catalytic RNA adopt its native structure, rather than to catalyze the underlying enzymatic reaction. These proteins function in part by altering the conformational dynamics of the RNA. In this work, we have used single-molecule FRET to monitor the conformational dynamics of the bI5 RNA prior to binding by the CBP2 cofactor, to probe the conformational transitions induced by CBP2 binding, and to observe the folding dynamics of the bI5 RNP.

Dynamic structure of the bI5 RNA

FRET trajectories reveal that the conformation of the bI5 RNA is dynamic. Distinct FRET levels are identified for several folding states of the bI5 RNA.^{10,35} The collapsed state at 7 mM Mg^{2+} is characterized by FRET=0.3 (Figure 3(a)). At lower Mg^{2+} concentrations where the RNA populates an expanded state, the FRET value decreases (Figure 3(c)). At higher Mg^{2+} concentrations where the bI5 core exhibits substantial native contacts, FRET is increased to 0.5 – 0.6 (Figure 3(b)). A similar FRET value is obtained when the core formation is facilitated by specific binding of CBP2 at 7 mM Mg^{2+} (Figure 4(a)). Docking of the P1-P2 domain into the core yields a FRET=0.8 (Figures 3(a) and (b), 4(a) and 9). The docking/undocking transitions of P1-P2 occur under all conditions, even at high concentrations of Mg^{2+} and CBP2 where the bI5 RNA is fully active (Figure 9 (a)) and at low concentrations of Mg^{2+} without CBP2 where the bI5 core is not folded and the RNA is inactive (Figure 3(a)).

Two distinct binding modes of CBP2 to its target RNA

CBP2 binds to its target RNA into distinct modes (Figures 4 and 10). The specific (type I) binding mode stabilizes the core structure formed between the P5-P4-P6 and P7-P3-P8 domains of the bI5 RNA and enhances the docking of the P1-P2 domain (Figure 4(a)). The non-specific (type II) mode induces highly dynamic conformational fluctuations

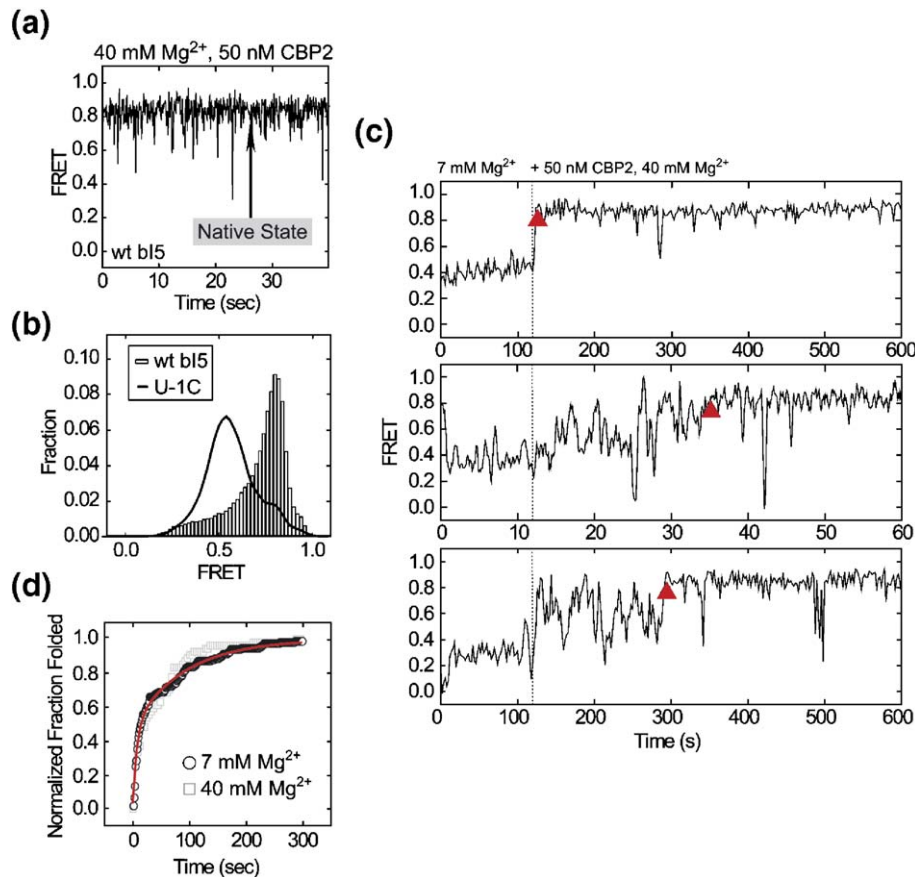


Figure 9. CBP2-assisted folding of bI5 occurs along multiple pathways that feature dynamic intermediate states. Single-molecule FRET trajectory (a) and histogram (b) illustrating the structural dynamics of a folded bI5 RNA molecule in 40 mM Mg^{2+} and 50 nM CBP2. A FRET histogram for the U-1C mutant is superimposed as a black line. (c) FRET traces depicting different folding kinetics and intermediate folding states for representative bI5 RNA molecules. The bI5 RNA was pre-incubated at 7 mM Mg^{2+} prior to buffer exchange into a folding buffer containing 40 mM Mg^{2+} and 50 nM CBP2 (dotted line). The upper and lower trajectories were collected at 0.5 Hz time resolution and the middle trajectory was collected at 10 Hz. The molecules often show a dynamic ensemble of intermediates states before attaining the native state, which is identified by a persistent high FRET state dwelling at 0.8 for at least 100 s except for brief excursions to lower FRET values due to P1-P2 undocking or Cy5 blinking. Red triangles indicate the attainment of the native state. (d) Fraction of the bI5 RNA molecules folded as a function of time after adding the folding buffer containing 40 mM Mg^{2+} and 50 nM CBP2. The starting conditions are 7 mM Mg^{2+} (circles) or 40 mM Mg^{2+} (squares) without CBP2. The folding kinetics at 7 mM Mg^{2+} were fit to equation (1), yielding folding rate constants $k_1 = 7.2 \text{ min}^{-1}$ and $k_2 = 0.54 \text{ min}^{-1}$. The overall fraction of molecules folded within the observation time is 65%, among which, the fractions of molecules folded with the faster and slower rates are 47% and 53%, respectively.

within the RNA, exemplified by fluctuations over a wide range of FRET values and several orders of magnitude in time scale (Figures 4(b) and 6). Furthermore, CBP2 has the ability to disrupt Watson-Crick base-pairs and to induce structural fluctuations in a simple RNA hairpin (Figure 7). These results indicate that CBP2 possesses an ability to destabilize RNA structures and induce conformational fluctuations within RNA. The apparent increase in conformational dynamics (or flexibility) may reflect stabilization of transition states on the RNA energy landscape by CBP2, which allow the RNA to access conformations that are kinetically inaccessible without CBP2. Alternatively, CBP2 may also stabilize the ground conformational states of the RNA that are otherwise insufficiently stable with dwell times too short for detection.

The protein-assisted bI5 RNA folding involves sequential non-specific and specific binding of CBP2

Single-molecule experiments show that CBP2 binds to the bI5 RNA rapidly, following bimolecular kinetics (Figure 8). This rapid association represents a fast-forming encounter complex mediated by non-specific, likely electrostatic, interactions. In contrast, experiments that preferentially score stable protein–RNA complexes show slow and unimolecular kinetics for the formation of stable bI5 RNA–CBP2 complex.^{19,20,40} Together, these results support a two-step binding model: CBP2 initially binds rapidly and non-specifically to the RNA; the conformational rearrangements in the RNA then allow stronger and more specific binding of CBP2

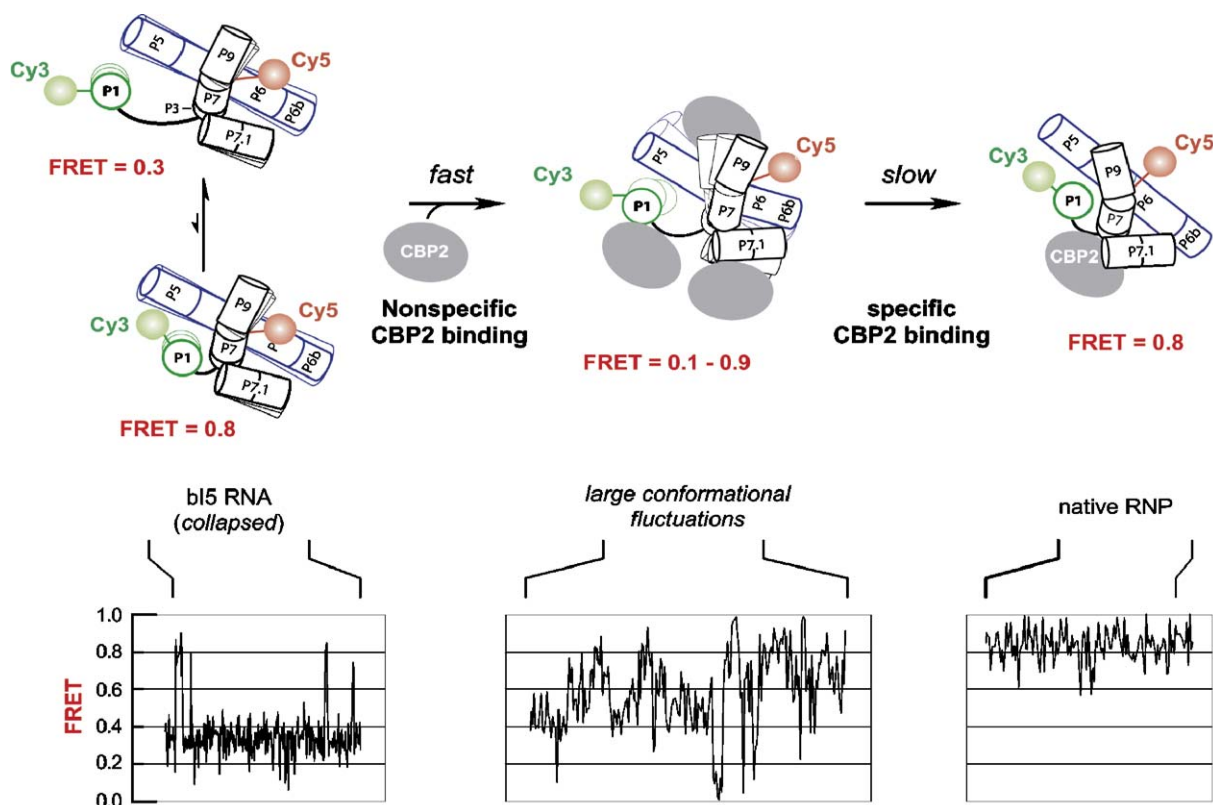


Figure 10. Sequential assembly model of the CBP2–bI5 RNA complex. In the absence of protein, the RNA is predominantly in a collapsed state and exhibits transient excursions to a more structured state with native-like features but without catalytic activity. Initial association of CBP2 with the RNA occurs rapidly in a non-specific mode that increases the local protein concentration and causes substantial conformational fluctuations in the RNA. Subsequent formation of specific CBP2–RNA interactions stabilizes the formation of the native structure of the bI5 RNA. Helices in the bI5 RNA are represented as cylinders. The view is looking down the P1 helix.²⁰ Representative FRET trajectories for each state illustrated in the lower panel are adapted from the data shown in Figures 3(a) and 9(c). Note that the CBP2–bI5 RNP folds along a multitude of pathways with distinct rate constants. In addition, a fraction of molecules misfold and do not attain native states in the observation time window. For clarity, these complex folding kinetics are not displayed in the model.

(Figure 10). As further support for the two-step binding picture, we directly observe that, at high concentrations of Mg^{2+} and CBP2, bI5 molecules fold into the native structure *via* dynamic intermediates similar to those induced by nonspecific CBP2 binding at lower Mg^{2+} concentrations (Figure 9(c)). Also consistent with the non-specific nature of the initial CBP2 binding, the bI5 molecules traverse multiple pathways as they fold towards the native state (Figure 9(c) and (d)).

While the specific binding mode of CBP2 stabilizes the native state of the bI5 RNA, what role(s) might the non-specific binding mode of CBP2 play in the assembly of the RNP? CBP2 has been suggested to assemble with the bI5 RNA *via* a tertiary structure capture mechanism.^{19,20} In this model, the protein cofactor does not direct the RNA to the native state, but rather binds to and stabilizes the RNA once the tertiary structure has transiently formed independent of the protein cofactor. Assembly of the native CBP2–bI5 RNP thus requires the coincidence of two rare events: transient formation of the RNA tertiary structure and a structurally productive collision between the RNA and the protein. The low

probability of these events occurring simultaneously could pose a challenge in efficient assembly of native RNP complexes. The rapid, non-specific binding of CBP2 to the bI5 RNA may alleviate this difficulty. By confining one or more CBP2 proteins to the vicinity of the RNA, non-specific binding effectively increases the local concentration of the protein cofactor, thus could potentially enhance the collision rate between the protein and the transiently formed RNA tertiary structure.

When bound non-specifically, CBP2 also increases the structural dynamics of the bI5 RNA (Figure 4) and transiently destabilizes RNA secondary structure (Figure 7), a property that has been proposed for RNA chaperones.^{13,17} This RNA structural-destabilizing activity likely arises from the electrostatic interactions between the negatively charged RNA and the positively charged domains of CBP2,⁴² which tend to destabilize RNA–RNA contacts to optimize RNA–protein contacts. It has been postulated that specific protein cofactors might first use non-specific electrostatic interactions to destabilize misfolded RNA structures, chaperoning the RNA to its native state, which is then

stabilized by specific protein–RNA interactions.¹⁷ Our results demonstrate that a specific protein cofactor can indeed possess an RNA structure destabilizing capability. Whether CBP2 indeed assists bI5 RNA folding by a chaperone mechanism in addition to tertiary structure stabilization awaits further investigation.

Methods

The bI5 RNA and CBP2 protein preparation

All fluorescently labeled RNA constructs consist of three oligonucleotides: an *in vitro* transcribed RNA that spans the majority of the bI5 sequence, plus two synthetic RNA or DNA oligonucleotides (Dharmacon and Qiagen Operon, respectively) labeled with Cy5 or Cy3. One of the oligonucleotides is also labeled with biotin to allow surface immobilization. The sequences used for each DNA or RNA oligo are listed in Table 1 of the Supplementary Data. Cy3 or Cy5 were either attached to the oligos during synthesis, or post-synthetically by conjugation of a mono-reactive dye (Amersham) to a primary amine group on the oligonucleotide. For all *in vitro* transcripts, DNA templates were PCR amplified from plasmid pTZ18U³³ and gel purified. The bI5 RNA transcript was annealed to the two synthetic strands in 50 mM Hepes (pH 7.6), 250 mM KCl and 1% (v/v) β -mercaptoethanol, and diluted in 40 mM MgCl₂, 50 mM Hepes (pH 7.6), 50 mM KCl, 10% (w/v) glucose, and 200 units/ml RNase inhibitor (Roche). CBP2 containing a C-terminal (His)₆ tag was purified from *Escherichia coli* by Ni²⁺-affinity chromatography, as described,³³ followed by cation exchange chromatography (Resource S column; Amersham Biosciences). The protein was dialyzed and stored in 20 mM Hepes (pH 7.6), 200 mM NaCl, 2 mM DTT and 50% (v/v) glycerol.

Surface immobilization of the bI5 RNA

Quartz slides were cleaned using argon plasma (Harrick Scientific), treated with 1% (w/v) Vectabond (Vector Laboratories) in acetone, rinsed, and incubated with a 20% (w/v) methoxy-PEG (*M_r* 5000; Nektar Therapeutics) and 0.2% biotin-PEG (*M_r* 3400 and 5000; Nektar Therapeutics) in 0.1 M sodium bicarbonate (pH 8.4) for at least 3 h. Streptavidin (0.2 mg/ml; Molecular Probes) in 50 mM Tris (pH 7.5) and 50 mM NaCl was applied before application of the biotinylated bI5 RNA diluted to 100–500 pM in a solution containing 50 mM Hepes (pH 7.6), 50 mM KCl, 10% glucose, and 40 mM MgCl₂.

Single-molecule FRET measurements

Donor and acceptor fluorescence from single bI5 molecules were separately resolved using a total internal reflection microscope, as described.²⁸ An Andor Ixon 887 back-illuminated electron multiplying CCD device was used to record the fluorescence image. The FRET value is defined as $I_A/(I_A+I_D)$, where I_A and I_D are the fluorescence signals detected from the acceptor and donor channel, respectively. Unless otherwise noted, all imaging buffers contained 50 mM KCl, 50 mM Hepes (pH 7.6), and 10% glucose, a variable amount of MgCl₂, and an oxygen

scavenger system (1% (v/v) β -mercaptoethanol, 300 μ g/ml of glucose oxidase, and 40 μ g/ml of catalase) to reduce photobleaching. All solutions containing CBP2 also contained 100–200 μ g/ml bovine serum albumin (BSA). Measurements were performed at room temperature.

Folding kinetics determination

Folding time for each molecule was defined as the time from addition of the folding buffer to the start of a stable FRET signal at 0.8 that lasts for at least 100 s. The cumulative folding time histogram was modeled by a double-exponential decay with two folding rate constants k_1 and k_2 , and an added contribution from photobleaching (with a rate constant k_p), which effectively biases against slow-folding molecules, as described by the following equation:

$$F = \frac{A_1 \left(\frac{k_1}{k_1+k_p} \right) (1 - e^{-(k_1+k_p)t}) + A_2 \left(\frac{k_2}{k_2+k_p} \right) (1 - e^{-(k_2+k_p)t})}{A_1 \left(\frac{k_1}{k_1+k_p} \right) + A_2 \left(\frac{k_2}{k_2+k_p} \right)} \quad (1)$$

where F is the normalized fraction of molecules folded to the native state, and A_1 and A_2 are the relative fractions of molecules exhibit folding rate constants k_1 and k_2 , respectively, with $A_1+A_2=1$. The photobleaching rate k_p was independently determined to be 0.06 min⁻¹.

Gel-based splicing assay

Splicing was performed by pre-incubating 5 nM fluorescently labeled bI5 RNA with 50 nM CBP2 in a buffer containing 50 mM Hepes (pH 7.6), 50 mM KCl, 7 or 40 mM MgCl₂, 0.1 mg/mL BSA, and 1% β -mercaptoethanol for more than 15 min, before splicing was initiated by the addition of GMP to 2 mM final concentration. The 15 μ l reaction aliquots were quenched with 5 μ l 500 mM EDTA and 100–200 units/ml of Proteinase K (Invitrogen). Reaction products were resolved on a native polyacrylamide gel and the Cy5 fluorescence intensities of the bands were quantified. Measurements of the splicing activity of non-labeled bI5 RNA (either with the unmodified DNA tether, or without any DNA tether) were performed by re-annealing Cy5-labeled DNA to the reaction products, for detection using a fluorescence-phosphorescence imager, after the splicing reaction had been quenched.

Acknowledgements

This work is supported in part by the Office of Naval Research, the National Science Foundation, a Packard Science and Engineering Fellowship, and the Howard Hughes Medical Institute (to X.Z.); and by the National Institutes of Health (GM 56222 to K.M.W.). G.B. is supported in part by a NIH training grant in Molecular, Cellular and Chemical Biology. L.G.N. is a Fannie and John Hertz pre-doctoral fellow.

Supplementary Data

Supplementary data associated with this article can be found, in the online version, at doi:10.1016/j.jmb.2006.06.048

References

1. Gesteland, R. F., Cech, T. R. & Atkins, J. F. (1999). *The RNA world*. 2nd edit., Cold Spring Harbor Laboratory Press, Cold Spring Harbor, NY.
2. Pan, J. & Woodson, S. A. (1998). Folding intermediates of a self-splicing RNA: Mispairing of the catalytic core. *J. Mol. Biol.* **280**, 597–609.
3. Pan, T. & Sosnick, T. R. (1997). Intermediates and kinetics traps in the folding of a large ribozyme revealed by circular dichroism and UV absorbance spectroscopies and catalytic activity. *Nature Struct. Biol.* **4**, 931–938.
4. Russell, R. & Herschlag, D. (1999). New pathways in folding of the *Tetrahymena* group I RNA enzyme. *J. Mol. Biol.* **291**, 1155–1167.
5. Treiber, D. K., Rook, M. S., Zarrinkar, P. P. & Williamson, J. R. (1998). Kinetic intermediates trapped by native interactions in RNA folding. *Science*, **279**, 1943–1946.
6. Zhuang, X., Bartley, L., Babcock, H., Russell, R., Ha, T., Herschlag, D. & Chu, S. (2000). A single molecule study of RNA catalysis and folding. *Science*, **288**, 2048–2051.
7. Onoa, B., Dumont, S., Liphardt, J., Smith, S. B., Tinoco, I. & Bustamante, C. (2003). Identifying kinetic barriers to mechanical unfolding of the T. thermophila ribozyme. *Science*, **299**, 1892–1895.
8. Sclavi, B., Sullivan, M., Chance, M. R., Brenowitz, M. & Woodson, S. A. (1998). RNA folding at millisecond intervals by synchrotron hydroxyl radical footprinting. *Science*, **279**, 1940–1943.
9. Treiber, D. K. & Williamson, J. R. (2001). Beyond kinetic traps in RNA folding. *Curr. Opin. Struct. Biol.* **11**, 309–314.
10. Weeks, K. M. & Cech, T. R. (1995). Protein facilitation of group I intron splicing by assembly of the catalytic core and the 5'-splice-site domain. *Cell*, **82**, 221–230.
11. Caprara, M. G., Lehnert, V., Lambowitz, A. M. & Westhof, E. (1996). A tyrosyl-tRNA synthetase recognizes a conserved tRNA-like structural motif in the group I intron catalytic core. *Cell*, **87**, 1135–1145.
12. Weeks, K. M. (1997). Protein-facilitated RNA folding. *Curr. Opin. Struct. Biol.* **7**, 336–342.
13. Schroeder, R., Grossberger, R., Pichler, A. & Waldsich, C. (2002). RNA folding *in vivo*. *Curr. Opin. Struct. Biol.* **12**, 296–300.
14. Hsien, J., Andrews, A. J. & Fierke, C. A. (2004). Roles of protein subunit in RNA-protein complexes: Lessons from Ribonuclease P. *Biopolymers*, **73**, 79–89.
15. Dreyfuss, G., Kim, V. N. & Kataoka, N. (2002). Messenger-RNA-binding proteins and the messages they carry. *Nat. Rev. Mol. Cell Biol.* **3**, 195–205.
16. Coetzee, T., Herschlag, D. & Belfort, M. (1994). *Escherichia coli* proteins, including ribosomal protein S12, facilitate *in vitro* splicing of phage T4 introns by acting as RNA chaperones. *Genes Dev.* **8**, 1575–1588.
17. Herschlag, D. (1995). RNA chaperones and the RNA folding problem. *J. Biol. Chem.* **270**, 20871–20874.
18. Caprara, M. G., Mohr, G. & Lambowitz, A. M. (1996). A tyrosyl-tRNA synthetase protein induces tertiary folding of the group I intron catalytic core. *J. Mol. Biol.* **257**, 512–531.
19. Weeks, K. M. & Cech, T. R. (1996). Assembly of a ribonucleoprotein catalyst by tertiary structure capture. *Science*, **271**, 345–348.
20. Garcia, I. & Weeks, K. M. (2004). Structural basis for the self-chaperoning function of an RNA collapsed state. *Biochemistry*, **43**, 15179–15186.
21. Geese, W. J. & Waring, R. B. (2001). A comprehensive characterization of a group IB intron and its encoded maturase reveals that protein-assisted splicing requires an almost intact intron RNA. *J. Mol. Biol.* **308**, 609–622.
22. Solem, A., Chatterjee, P. & Caprara, M. G. (2002). A novel mechanism for protein-assisted group I intron splicing. *RNA*, **8**, 412–425.
23. Mohr, S., Stryker, J. M. & Lambowitz, A. M. (2002). A DEAD-box protein functions as an ATP-dependent RNA chaperone in group I intron splicing. *Cell*, **109**, 769–779.
24. Selvin, P. R. (1995). Fluorescence resonance energy-transfer. *Methods Enzymol.* **246**, 300–334.
25. Weiss, S. (2000). Measuring conformational dynamics of biomolecules by single molecule fluorescence spectroscopy. *Nature Struct. Biol.* **7**, 724–729.
26. Ha, T., Zhuang, X., Kim, H., Orr, J. W., Williamson, J. R. & Chu, S. (1999). Ligand-induced conformational changes observed in single RNA molecules. *Proc. Natl Acad. Sci. USA*, **96**, 9077–9082.
27. Cosa, G., Zeng, Y. N., Liu, H. W., Landes, C. F., Makarov, D. E., Musier-Forsyth, K. & Barbara, P. F. (2006). Evidence for non-two-state kinetics in the nucleocapsid protein chaperoned opening of DNA hairpins. *J. Phys. Chem. B*, **110**, 2419–2426.
28. Zhuang, X., Kim, H., Pereira, M., Babcock, H., Walter, N. & Chu, S. (2002). Correlating structural dynamics and function in single ribozyme molecules. *Science*, **296**, 1473–1476.
29. Tan, E., Wilson, T. J., Nahas, M. K., Clegg, R. M., Lilley, D. M. J. & Ha, T. (2003). A four-way junction accelerates hairpin ribozyme folding via a discrete intermediate. *Proc. Natl Acad. Sci. USA*, **100**, 9308–9313.
30. Xie, Z., Srividya, N., Sosnick, T. R., Pan, T. & Scherer, N. F. (2004). Single-molecule studies highlight conformational heterogeneity in the early folding steps of a large ribozyme. *Proc. Natl Acad. Sci. USA*, **101**, 534–539.
31. Lipman, E. A., Schuler, B., Bakajin, O. & Eaton, W. A. (2003). Single-molecule measurement of protein folding kinetics. *Science*, **301**, 1233–1235.
32. Gampel, A. & Tzagoloff, A. (1987). *In vitro* splicing of the terminal intervening sequence of *Saccharomyces cerevisiae* cytochrome-B pre-mRNA. *Mol. Cell Biol.* **7**, 2545–2551.
33. Weeks, K. M. & Cech, T. R. (1995). Efficient protein-facilitated splicing of the Yeast mitochondrial bI5 intron. *Biochemistry*, **34**, 7728–7738.
34. Shaw, L. C. & Lewin, A. S. (1995). Protein-induced folding of a group I intron in cytochrome *b* pre-mRNA. *J. Biol. Chem.* **270**, 21552–21562.
35. Buchmueller, K. L., Webb, A. E., Richardson, D. A. & Weeks, K. M. (2000). A collapsed non-native RNA folding state. *Nature Struct. Biol.* **7**, 362–366.
36. Mrksich, M. & Whitesides, G. M. (1997). Using self-assembled monolayers that present oligo(ethylene glycol) groups to control the interactions of proteins with surfaces. *ACS Symposium Series*, **680**, 361–373.
37. Knitt, D. S., Narlikar, G. J. & Herschlag, D. (1994). Dissection of the role of the conserved GU pair in group I RNA self-splicing. *Biochemistry*, **33**, 13864–13879.
38. Chamberlin, S. I. & Weeks, K. M. (2003). Differential helix stabilities and sites pre-organized for tertiary interactions revealed by monitoring local nucleotide flexibility in the bI5 group I intron RNA. *Biochemistry*, **42**, 901–909.

39. Buchmueller, K. L. & Weeks, K. M. (2003). Near native structure in an RNA collapsed state. *Biochemistry*, **42**, 13869–13878.
40. Webb, A. E. & Weeks, K. M. (2001). A collapsed state functions to self-chaperone RNA folding into a native ribonucleoprotein complex. *Nature Struct. Biol.* **8**, 135–140.
41. Webb, A. E., Rose, M. A., Westhof, E. & Weeks, K. M. (2001). Protein-dependent transition states for ribonucleoprotein assembly. *J. Mol. Biol.* **309**, 1087–1100.
42. Tirupati, H. K., Shaw, L. C. & Lewin, A. S. (1999). An RNA binding motif in the Cbp2 protein required for protein-stimulated RNA catalysis. *J. Biol. Chem.* **274**, 30393–30401.

Edited by D. E. Draper

(Received 7 May 2006; received in revised form 18 June 2006; accepted 19 June 2006)
Available online 7 July 2006